Enhancement of Be and Mg incorporation in wurtzite quaternary BeMgZnO alloys with up to 5.1 eV optical bandgap

M. Toporkov,[1] V. Avrutin,[1] S. Okur,[1] N. Izyumskaya,[1] D. Demchenko,[2] J. Volk,[1,3] D. J. Smith,[4] H. Morkoç,[1] and Ü. Özgür[1]

[1] Department of Electrical and Computer Engineering, Virginia Commonwealth University, Richmond, VA

[2] Department of Physics, Virginia Commonwealth University, Richmond, VA

[3] Research Centre for Natural Sciences, Institute for Technical Physics and Materials Science, Hungarian Academy of Sciences, Budapest, Hungary

[4] Department of Physics, Arizona State University, Tempe, AZ

A wide range of optical bandgap modulation up to 5.1 eV was achieved for quaternary BeMgZnO thin films prepared using plasma assisted molecular beam epitaxy, enabling development of UV emitters and solar-blind photodetectors. The significantly improved structural quality and bandgap widening in BeMgZnO layers as compared to BeZnO and MgZnO ternaries indicate enhanced incorporation of both Be and Mg on Zn sites in the wurtzite lattice. Correlation of lattice parameters with optical bandgaps reveals that co-alloying MgO and BeO with ZnO helps overcome the impediment of limited bandgap extension offered by the corresponding ternary compounds due to phase separation and allows lattice-matched or nearly

lattice-matched BeMgZnO/ZnO heterostructures. Optimization of growth conditions at higher Mg and/or Be fluxes is expected to provide bandgaps beyond 5.1 eV.

1. Introduction

ZnO is a highly attractive semiconductor material for light emitter and detector applications owing to its large exciton binding energy and wide direct bandgap.[1,2] For some device applications, ZnO-based materials with wider bandgap are highly desired. For instance, solar-blind UV detectors are required to have a cut-off wavelength below 280 nm, which corresponds to a bandgap value of 4.5 eV. Alloying with MgO (7.8 eV bandgap) is conventionally used to increase the bandgap. However, although it has been studied extensively over the last 20 years, ternary MgZnO alloy provides limited bandgap tuning in the wurtzite phase (wurtzite MgO bandgap 7.16 eV)[3] due to fact that MgO has a cubic rocksalt lattice. Consequently, phase segregation becomes inevitable as the Mg content of the ZnMgO solid solution increases. Ohtomo *et al.*[4] and Sharma *et al.*[5] were able to tune the bandgap to ~4 eV for wurtzite MgZnO alloys containing 33% and 36% Mg, respectively. The second-phase formation at higher Mg contents could be suppressed at low growth temperatures but at the expense of inferior material quality: 55% Mg incorporation to ZnO in wurtzite phase and a corresponding absorption edge of 4.55 eV have been achieved by Du *et al.*[6] using plasma assisted molecular beam epitaxy (MBE) at a substrate temperature of 250 °C. It has been also possible to achieve metastable cubic phase MgZnO with even higher Mg content by mainly reducing the growth temperature.[7] Caveat in this case, however, is the loss of semiconductor functionally (the cubic material is an insulator rather than semiconductor). It should also be noted that supersaturated solid solutions are unstable against exposure to elevated temperatures during thermal treatments or device operation, which can trigger the second-phase formation and limit their practical use.

The alternative BeZnO ternary alloy has been proposed[8] to be more advantageous compared to MgZnO as it is expected to maintain the wurtzite structure for the whole

compositional range, and therefore, provide a wide range of bandgap tuning potentially up to that of BeO (10.6 eV). However, despite the initial optimistic report of bandgap modulation up to 5.4 eV8 in BeZnO, recent studies[9,10] indicate that $Be_xZn_{1-x}O$ solid solutions with intermediate Be composition are unstable and segregate into low- and high-Be content phases due to the large lattice mismatch of the binary constituents and large covalent radii difference between Zn and Be (1.22 Å for Zn, 0.96 Å for Be[11]), making it difficult to incorporate intermediate concentrations of Be to the ZnO lattice.[9,10,12] In order to overcome this limitation, BeMgZnO quaternary alloy has been considered,[13,14,15] but with little or no emphasis on structural details and lattice parameters. One major advantage of this quaternary system is that Mg has a much larger covalent radius (1.41 Å[11]) than Be and thus can compensate for the large lattice mismatch between ZnO and BeO and lead to better crystal quality. This also opens a possibility for tuning quaternary composition to maintain lattice matching to ZnO while extending the bandgap into the solar blind region. The largest bandgap values achieved so far for BeMgZnO are 4.5 and 4.9 eV for plasma-assisted MBE[14] and PLD[13] grown material, respectively.

Here, we report on a systematic investigation of lattice parameters and optical bandgap values, E_g, of the BeMgZnO layers grown by rf-plasma-assisted MBE on *c*-sapphire substrates. X-ray diffraction analysis indicates that co-doping with Be and Mg increases incorporation of both Be and Mg into the wurtzite ZnO lattice, which allows us to achieve optical bandgaps as large as 5.11 eV. The quaternary compound BeMgZnO is also found to exhibit better structural quality compared to ternary BeZnO with similar Be content.

2. Experimental procedure

Quaternary BeMgZnO thin films were grown on (0001) sapphire substrates using plasma assisted MBE with an RF oxygen plasma source and Knudsen cells for Zn, Be and Mg. PBN

crucibles were used for Zn and Mg sources and a BeO crucible for the Be source. First, a 2nm-thick MgO buffer layer was grown at 700°C to ensure 2D nucleation. Subsequently, an ~ 8nm-thick low-temperature ZnO (LT-ZnO) buffer layer was grown at 300°C and annealed at 700°C to achieve an atomically flat surface. BeMgZnO films (samples C1-C6) were deposited at ~8 x 10^{-6} Torr oxygen pressure, 400 W RF plasma power, and 400°C substrate temperature, which was found to be optimal for the best crystal quality and reasonable Be incorporation (up to 10%). In addition, one MgZnO layer (sample A) and three BeZnO layers (samples B1, B2, B3) of various compositions were grown at the same substrate temperature of 400°C. The growth rate was ~ 100 nm/h, and the film thicknesses were 150-200 nm (determined from step profilometer measurements). The compositions of the ternary and quaternary samples were estimated from deposition rates of binary oxides BeO, MgO, and ZnO measured by an Inficon quartz monitor and the calibration provided from elastic proton backscattering measurements on selected samples (B2, C1, C5, C6, and an additional sample with composition similar to C3 but grown at 375°C substrate temperature). It is worth mentioning that elastic proton backscattering measurements account for the total atomic concentrations in the films, regardless of the atoms' positions in the lattice. To change the quaternary alloy composition, the Mg source temperature T_{Mg} was varied from 416 to 452 °C, while the Be source temperature T_{Be} was kept at 1150°C and the Zn source temperature T_{Zn} at either 324°C or 320°C. The growth progression and to some extent the structural quality of the samples were monitored *in situ* by using Reflection High-Energy Electron Diffraction (RHEED). The *c*- and *a*-lattice parameters were deduced from X-Ray Diffraction (XRD) measurements for the symmetric (0002) and skew-symmetric (10-13) reflections, respectively, using the line focus mode. The optical absorption measurements were

performed using a Deuterium lamp and a SPEX 500M scanning spectrometer equipped with a photomultiplier tube.

3. Results and discussion

Table I lists compositions, temperatures of the Be, Mg, and Zn sources, out-of-plane c and in-plane a lattice parameters, cell volumes, and optical bandgap values for the studied samples. Series B samples of BeZnO were grown at the same Zn cell temperature ($T_{Zn}=324°C$), but with various Be cell temperatures. The bandgap of BeZnO rises from 3.45 to 3.54 eV with increasing T_{Be} from 1140 to 1150 °C. However, further increase of T_{Be} to 1160 °C results in very small increase in E_g from 3.54 to 3.57 eV, which suggests that incorporation of Be into the ZnO lattice has saturated for sample B3 grown with $T_{Be}=1160$ ºC. This finding is in accord with Chen $et\ al.$,[9] who reported that the bandgap of BeZnO first increases with Be content up to 8% Be but then saturates and even slightly decreases as the Be content is increased further to 36%. This behavior may be attributed to either phase separation[9,10,12] or incorporation of Be on interstitial positions.[16] Consequently, in this study, the Be cell temperature was chosen as 1150°C to avoid saturation of Be content for the series C BeMgZnO samples.

BeMgZnO samples C1, C2, C3, and C5 were grown at the same $T_{Zn} = 324°C$, but with different Mg cell temperatures. As seen from Fig. 1 and Table I, as T_{Zn} increases from 416 to 452°C (corresponding Mg content increases from 16 to 50%) the bandgap widens from 3.90 to 4.77 eV. It is worth noting that BeZnO sample B2 grown with the same Be cell temperature of 1150 °C as the BeMgZnO samples has a much smaller optical bandgap of 3.54 eV. Moreover, the bandgap of MgZnO sample A is also smaller than that of sample C3 (3.72 eV vs. 4.16 eV), which is grown using the same Mg cell temperature of 440°C, but contains both Be and Mg.

Samples C3 and C4 were grown at the same T_{Be} = 1150 °C and T_{Mg} ~ 440°C but with different T_{Zn}, 324 and 320°C, respectively. For sample C4, the Zn cell temperature was decreased to reduce the Zn content, and consequently, increase Mg and Be content of the sample, which should result in wider bandgap. Indeed, the bandgap of sample C4 is much higher than that of sample C3 (4.63 eV vs. 4.16 eV). Sample C6 was grown also with T_{Zn} = 320°C and T_{Be} = 1150°C, but increased T_{Mg} of 444°C. As a result, the bandgap further increased to 5.11 eV, which far exceeds the values obtained for the ternary compounds (see Table I and Fig. 1). Further advantages of co-alloying ZnO with both BeO and MgO is discussed in more detail below.

Figure 2 shows the typical RHEED patterns of the BeZnO and BeMgZnO samples. The ZnO buffer layer exhibits a clear streaky pattern after the annealing stage [Fig. 2(a), Fig. 2(b)], indicative of an atomically flat surface. As the BeMgZnO deposition is initiated, a rapid transition to a spotty pattern indicative three-dimensional (3D) growth mode emerges, and nearly no further change occurs during the rest of the 86 min growth [Fig. 2(d)]. Moreover, despite the rapid transition from 2D to 3D growth mode, the pattern retains some elongation of reflection spots indicating flatter surface morphology compared to that of BeZnO, which exhibited arc-like broadening as shown in Fig. 2(c). Similar RHEED pattern of BeZnO has been observed by Chen *et al.*[9] In the case of relatively high substrate temperatures (>500°C), extra reflections corresponding to BeO or BeO-rich phases were clearly observed in the RHEED patterns (not shown) for BeZnO ternary. These RHEED observations, therefore, suggest that incorporation of Mg along with Be into the ZnO lattice improves the crystallinity of the quaternary material.

The RHEED observations are supported by the XRD data. Figure 3 shows the XRD 2θ-ω scans for the symmetric (0002) reflections from MgZnO (sample A), BeZnO (sample B2), BeMgZnO layers C1, C2, C3, and C5 grown with Mg-cell temperature varying from 416 °C to

452$^{\text{o}}$C, which correspond to Mg concentrations from 16% to 50%, and BeMgZnO layers C4 and C6 grown with reduced Zn-cell temperature compared to others. The peak intensity first increases with Mg flux, reaching a maximum for sample C3 grown with T_{Mg}=440$^{\text{o}}$C. Further increase in Mg content (samples C4, C5, and C6) broadens the linewidth and decreases the intensity of the XRD peak, which suggest increasing lattice disorder. It should be noted that all the BeMgZnO layers exhibit substantially better crystal quality than BeZnO as can be surmised from the higher peak intensities and narrower reflection lines. For example, with incorporation of Mg, the XRD peak intensity of sample C1 increases by about three times compared to that of Sample B2. The Mg/Be composition ratio for sample C3 featured by the highest structural quality is about 4.3. However, the same ratio may not provide the best material quality for higher Be content samples, as the formation of the second phase driven by very large mismatch in covalent radii of Mg and Be cannot be ruled out. Additionally, different bowing can be expected in the compositional dependence of lattice parameters in the case of Zn substitution with Be and Mg, thus, also possibly resulting in different optimum Be-to-Mg ratios for different concentration ranges.

Figure 4(a) shows the out-of-plane c lattice parameters determined from the symmetrical XRD scans using the sapphire (0006) reflection as a reference versus the optical bandgap together with those available in the literature for MgZnO,[4] BeZnO,[17] and BeMgZnO.[13] As seen from Fig. 4(a), the c parameter of the quaternary BeMgZnO alloys (solid circles) shows substantial decrease with increasing Mg content similar to that reported by Ohtomo *et al*.[4] for MgZnO (open stars). However, the whole dependence is shifted to much lower c values apparently due to the presence of Be with smaller covalent radius. Yang *et al.*[13] reported a

similar variation of the *c* parameters within the same range [open circles in Fig. 4(a)] for the BeMgZnO layers grown at constant Mg but varying Be flux.

Figure 4(b) presents in-plane *a*-lattice parameters for the BeMgZnO, BeZnO, and MgZnO alloys obtained in this study together with literature data for MgZnO 4 and BeZnO.[17] The *a* parameters were calculated from skew-symmetric (10-13) XRD scans with the use the *c*-lattice parameters shown in Fig. 4 (a). In contrast to large variation of out-of-plane *c* parameters with composition, relatively small variation (from 3.210 to 3.255 Å) is observed for the in-plane lattice parameters of BeMgZnO. Note that samples C2 and C3, which have in-plane lattice parameters very close to the ZnO template, also exhibit the highest intensities and narrowest linewidths for XRD peaks among all the structures studies (Fig. 3). It is worth noting that samples C1 to C3 exhibit "MgZnO-like" dependence, i.e. the *a* parameter increases with increasing Mg content (see also Table I). However, for samples from C4 to C6 the increase in the band gap correlates with the decrease in *a* parameter. As seen from Fig. 5, the relationship between the cell volume and optical bandgap of the quaternary BeMgZnO alloys behaves in a similar way. In the series of samples from C1 to C3, the bandgap and the cell volume increase with increasing Mg content. However, for samples C4, C5, and C6 with higher Mg contents (see Table I), the increase in E_g correlates with a drastic decrease in the cell volume. For sample C6, which exhibits the widest bandgap, both *c* and *a* parameters are the smallest. The rapid decrease of the *a*-parameter and the cell volume of BeMgZnO alloys with increasing Mg content observed for samples C4, C5, and C6 (Table I) cannot be explained only by increasing Mg concentration. We may presume that increasing Mg content enhances substitution of Be on Zn lattice sites, rather than possible presence of Be interstitials and/or Be-rich inclusions. However, an alternative scenario involving formation of Be-poor phase within Be-rich matrix cannot be

9

completely ruled out. The low-angle shoulder of BeZnMgO (0002) reflection at around $2\theta = 35.3°$ for the structures with the highest Mg content (samples C4, C5, and C6,) may be indicative of the Be-poor phase. The driving force for such separation would be large difference in covalent radii of Be and Mg as indicated before. The Be-rich matrix corresponding to the dominating XRD reflection would have a lower cell volume and wider bandgap. Further insight into incorporation of Be and Mg on Zn sites in wurtzite BeMgZnO can be gained by correlation of experimental observations inclusive of high resolution microscopy and ion channeling experiments with accurate theoretical calculations of lattice parameters and bandgaps.

4. Conclusions

Optical bandgaps up to 5.11 eV were achieved for quaternary BeMgZnO alloys. The results of structural studies correlated with optical bandgaps suggest that co-alloying with Be and Mg increase incorporation of both Be and Mg into the wurtzite ZnO lattice. The quaternary BeMgZnO system provides a wider range of bandgap modulation as compared to ternary BeZnO or MgZnO compounds with an additional benefit of higher crystal quality than that of BeZnO. Co-alloying MgO and BeO with ZnO helps overcome the impediment of limited bandgap extension offered by these ternaries due to phase separation and allows production of lattice-matched or nearly lattice-matched BeMgZnO/ZnO heterostructures. In overall, due to its lattice matching to ZnO and wide bandgap, the BeMgZnO quaternary material is shown to have great potential for heterostructure devices inclusive of UV emitters and solar blind photodetectors.

References

[1] H. Morkoç and Ü. Özgür, Zinc oxide: fundamentals, materials and device technology, Wiley-VCH, Weinheim, 2009.

[2] Ü. Özgür, Y.I. Alivov, C. Liu, A. Teke, M.A. Reshchikov, S. Doğan, V. Avrutin, S. –J. Cho, and H. Morkoç, J. Appl. Phys. **98**, 041301 (2005).

[3] Q. Yan, P. Rinke, M. Winkelnkemper, A. Qteish, D. Bimberg, M. Scheffler, and C.G. Van de Walle, Appl. Phys. Lett. **101**, 152105 (2012).

[4] A. Ohtomo, M. Kawasaki, T. Koida, K. Masubuchi, H. Koinuma, Y. Sakurai, Y. Yoshida, T. Yasuda, and Y. Segawa, Appl. Phys. Lett. **72**, 2466 (1998).

[5] A. K. Sharma, J. Narayan, J. F. Muth, C. W. Teng, C. Jin, A. Kvit, R. M. Kolbas, and O. W. Holland, Appl. Phys. Lett. **75,** 3327 (1999).

[6] X. L. Du, Z. X. Mei, Z. L. Liu, Y. Guo, T. C. Zhang, Y. N. Hou, Z. Zhang, Q. K. Xue, and A. Y. Kuznetsov, Adv. Mater. **21,** 4625 (2009).

[7] S. Choopun, R.D. Vispute, W. Yang, R.P. Sharma, T. Venkatesan, and H. Shen, Appl. Phys. Lett. **80**, 1529 (2002).

[8] Y.R. Ryu, T.S. Lee, J.A. Lubguban, A.B. Corman, H.W. White, J.H. Leem, M.S. Han, Y.S. Park, C.J. Youn, and W.J. Kim, Appl. Phys. Lett. **88**, 052103 (2006).

[9] M. Chen, Y. Zhu, L. Su, Q. Zhang, A. Chen, X. Ji, R. Xiang, X. Gui, T. Wu, B. Pan, and Z. Tang, Appl. Phys. Lett. **102**, 202103 (2013).

[10] L. Su, Y. Zhu, M. Chen, Q. Zhang, Y. Su, X. Ji, T. Wu, X. Gui, R. Xiang, and Z. Tang, Appl. Phys. Lett. **103**, 072104 (2013).

[11] B. Cordero, V. Gómez, A.E. Platero-Prats, M. Revés, J. Echeverría, E. Cremades, F. Barragán, and S. Alvarez, Dalton Trans. **21,** 2832 (2008).

[12] C.K. Gan, X.F. Fan, and J.-L. Kuo, Comput. Mater. Sci. **49**, S29 (2010).

[13] C. Yang, X.M. Li, Y.F. Gu, W.D. Yu, X.D. Gao, and Y.W. Zhang, Appl. Phys. Lett. **93**, 112114 (2008).

[14] L. Su, Y. Zhu, Q. Zhang, M. Chen, X. Ji, T. Wu, X. Gui, B. Pan, R. Xiang, and Z. Tang, J. Phys. Appl. Phys. **46**, 245103 (2013).

[15] C. Yang, X.M. Li, X.D. Gao, X. Cao, R. Yang, and Y.Z. Li, J. Cryst. Growth **312**, 978 (2010).

[16] F.T. Kong and H.R. Gong, Comput. Mater. Sci. **61**, 127 (2012).

[17] W.J. Kim, J.H. Leem, M.S. Han, I.-W. Park, Y.R. Ryu, and T.S. Lee, J. Appl. Phys. **99**, 096104 (2006).

Figure captions.

Table captions:

TABLE I. Compositions, metal source temperatures, lattice parameters c and a, cell volume, and optical bandgap, E_g, for the studied samples. The compositions of samples B2, C1, C5, and C6 were determined from elastic proton backscattering measurements.
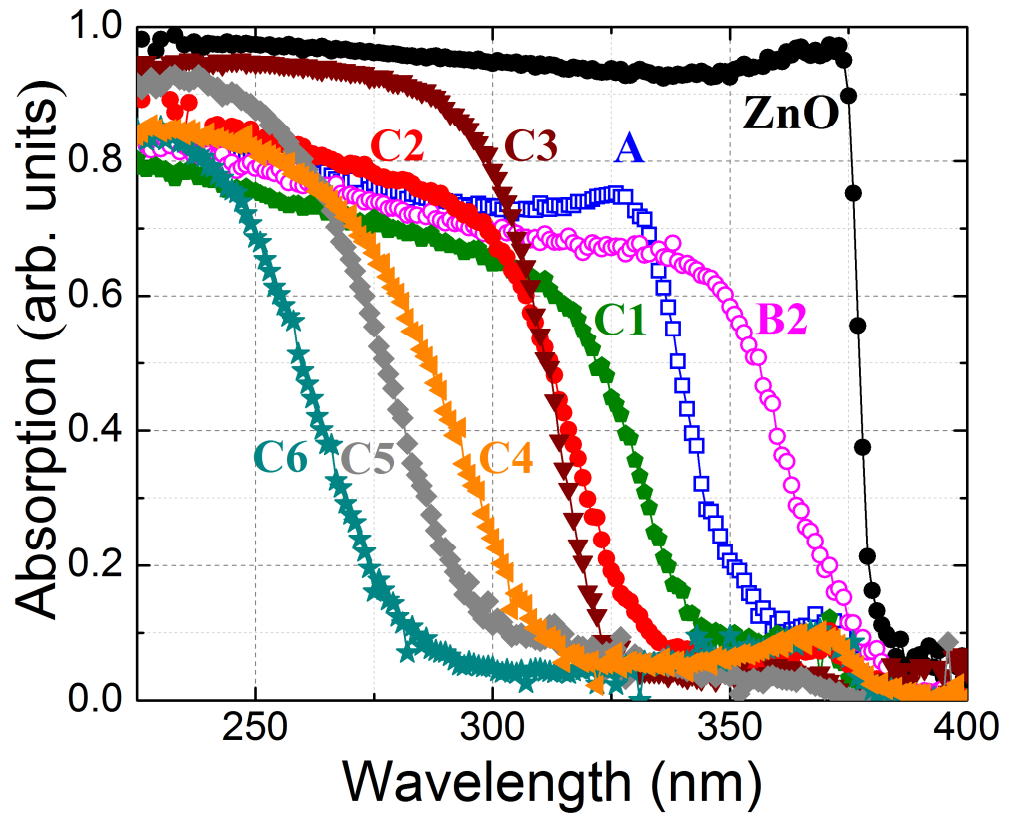
Figure captions:

FIG.1. Room temperature optical absorption spectra of ZnO, MgZnO, BeZnO and BeMgZnO thin films. Note that $\lambda < 280$ nm corresponds to the solar-blind spectral region.
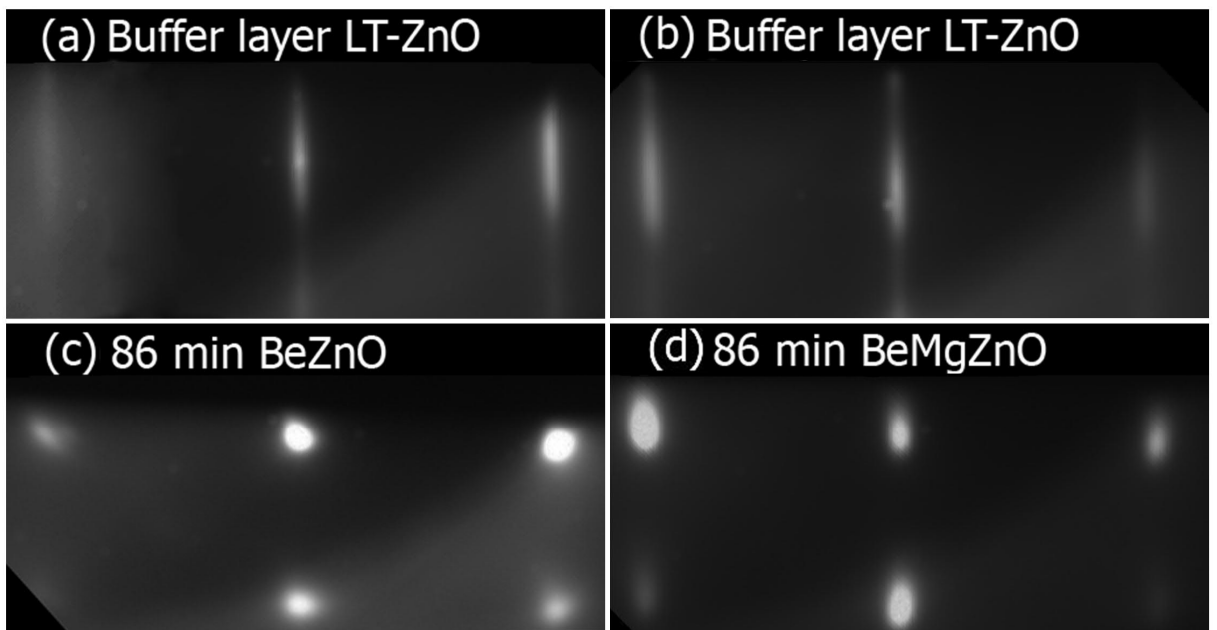
FIG.2. RHEED patterns of (a) and (b) ZnO buffer layers after annealing at 700ºC, (c) BeZnO layer (sample B2) after 86 min of growth and (d) BeMgZnO layer (sample C3) after 86 min of growth.
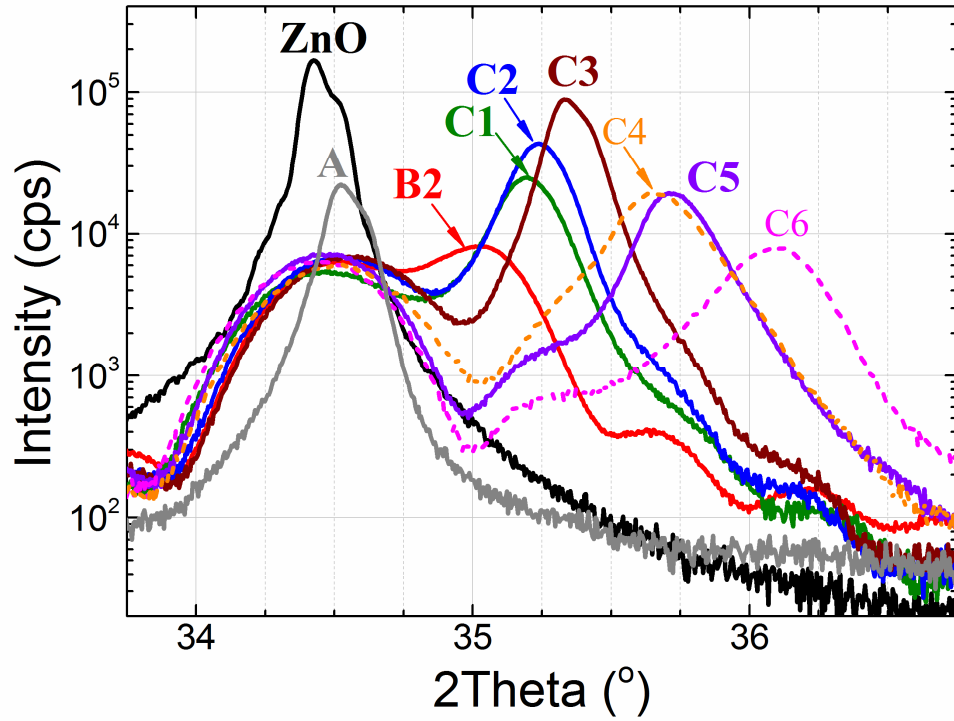
FIG. 3. Symmetric XRD 2theta-Omega scans for the (0002) reflection of MgZnO (sample A), BeZnO (sample B2), and BeMgZnO (samples C1-C6), compared with that of a reference ZnO sample.
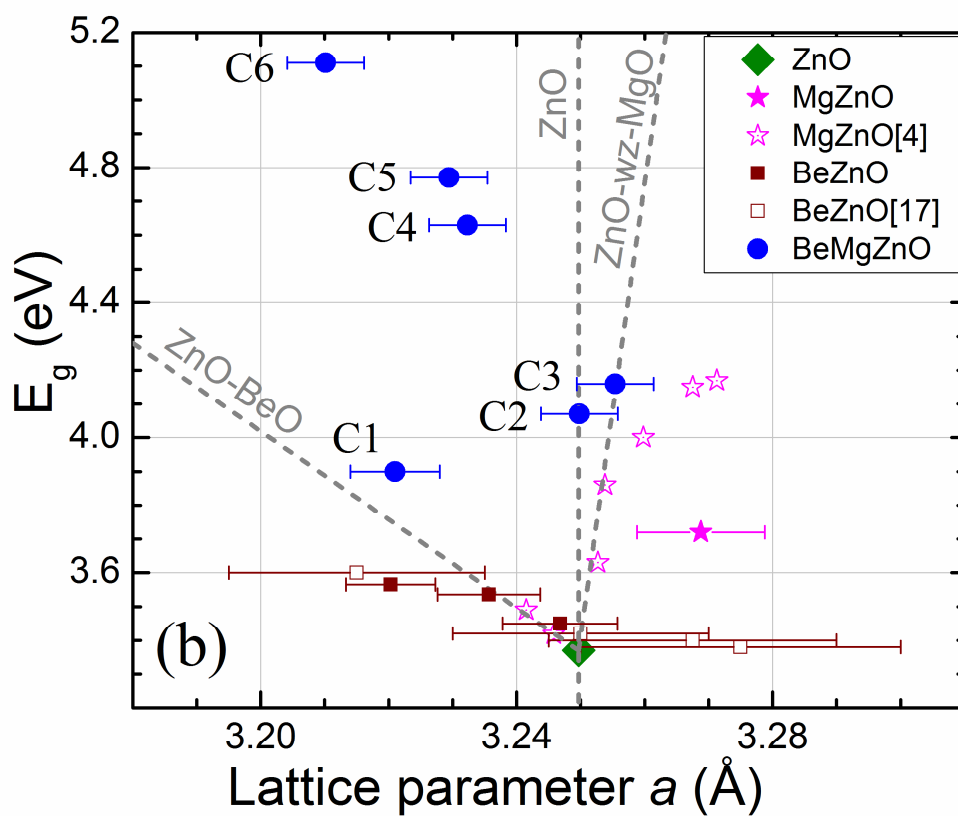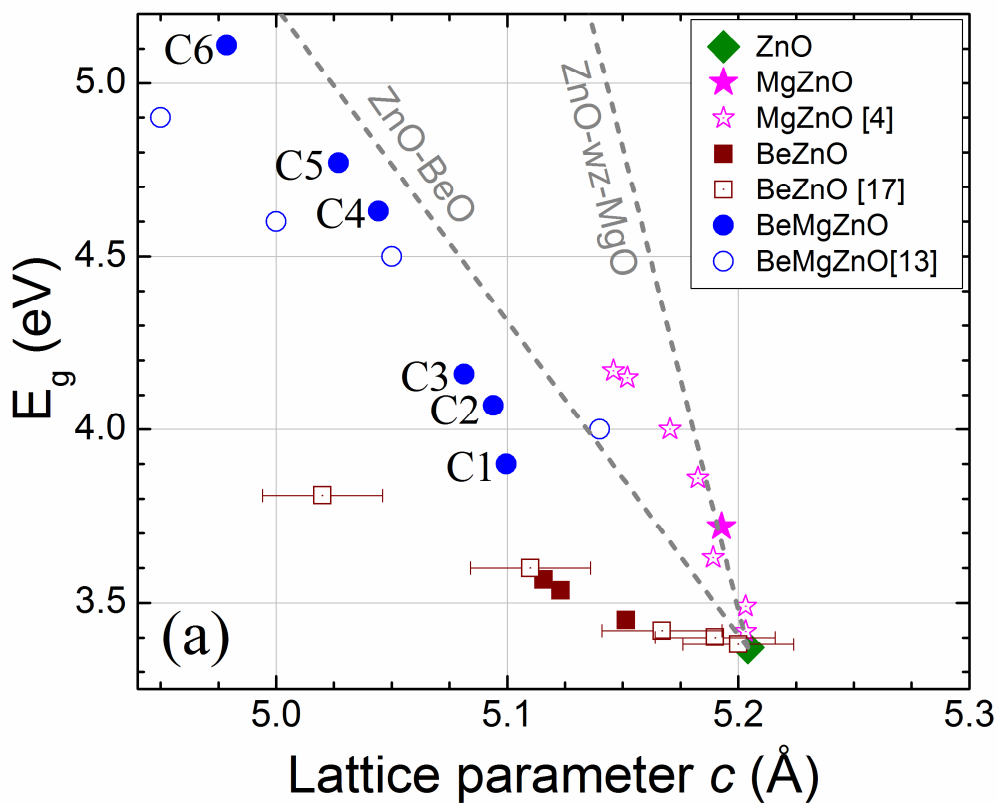
FIG. 4. Optical bandgap energy versus (a) the out-of plane c lattice parameter and (b) the in-plane a lattice parameter for the BeMgZnO, BeZnO, and MgZnO samples investigated here. Data from literature are also included for comparison. Dashed lines represent the linear interpolations between wurtzite ZnO-BeO and ZnO - hypothetical wurtzite MgO binaries. [3]
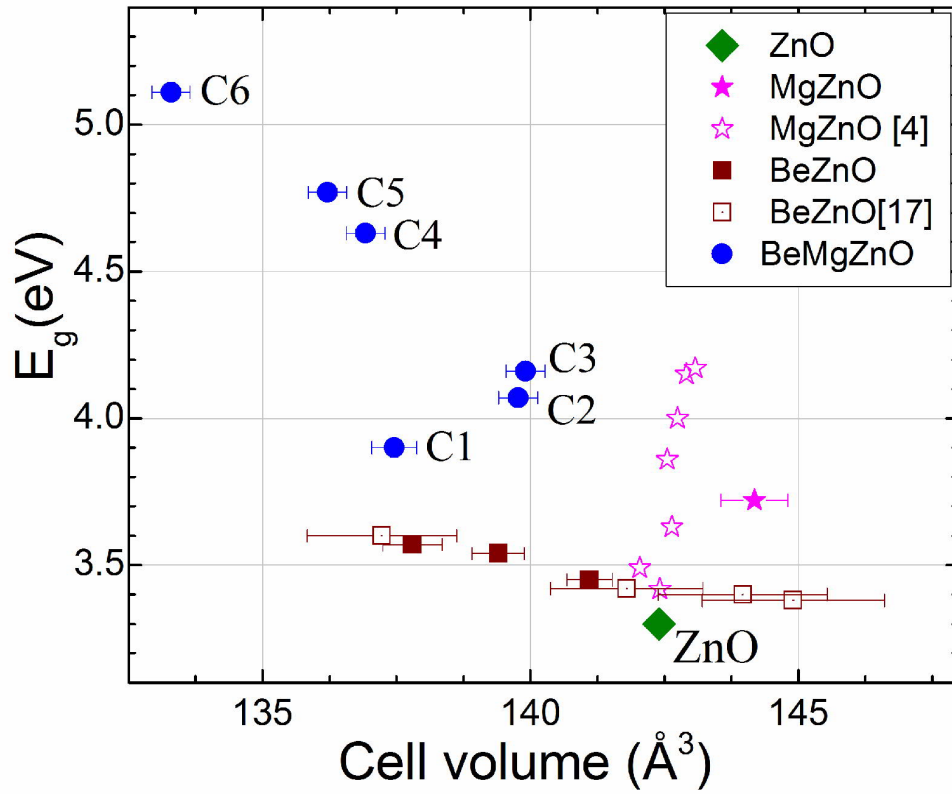

FIG. 5. Optical bandgap energy versus cell volume for BeMgZnO, BeZnO and MgZnO samples. Data from literature are also included for comparison.

Tables:

TABLE I.

Sample	Composition	$T_{Zn,}$ °C	$T_{Mg,}$ °C	$T_{Be,}$ °C	c, Å	a, Å	Cell volume, Å³	$E_{g,}$ eV
A	$Mg_{0.39}Zn_{0.61}O$	324	440	-	5.193	3.269	144.2	3.72
B1	$Be_{0.09}Zn_{0.91}O$	324	-	1140	5.151	3.247	141.1	3.45
B2	$Be_{0.10}Zn_{0.90}O$	324	-	1150	5.123	3.236	139.4	3.54
B3	$Be_{0.14}Zn_{0.86}O$	324	-	1160	5.116	3.220	137.8	3.57
C1	$Be_{0.09}Mg_{0.16}Zn_{0.75}O$	324	416	1150	5.100	3.221	137.5	3.90
C2	$Be_{0.08}Mg_{0.23}Zn_{0.69}O$	324	426	1150	5.094	3.250	139.8	4.07
C3	$Be_{0.07}Mg_{0.30}Zn_{0.63}O$	324	440	1150	5.081	3.255	139.9	4.16
C4	$Be_{0.08}Mg_{0.40}Zn_{0.52}O$	320	438	1150	5.044	3.232	136.9	4.63
C5	$Be_{0.05}Mg_{0.50}Zn_{0.45}O$	324	452	1150	5.027	3.229	136.2	4.77
C6	$Be_{0.08}Mg_{0.52}Zn_{0.40}O$	320	444	1150	4.979	3.210	133.3	5.11